Soft Matter

Accepted Manuscript

This is an *Accepted Manuscript*, which has been through the Royal Society of Chemistry peer review process and has been accepted for publication.

Accepted Manuscripts are published online shortly after acceptance, before technical editing, formatting and proof reading. Using this free service, authors can make their results available to the community, in citable form, before we publish the edited article. We will replace this *Accepted Manuscript* with the edited and formatted *Advance Article* as soon as it is available.

You can find more information about *Accepted Manuscripts* in the Information for Authors.

Please note that technical editing may introduce minor changes to the text and/or graphics, which may alter content. The journal's standard Terms & Conditions and the Ethical guidelines still apply. In no event shall the Royal Society of Chemistry be held responsible for any errors or omissions in this *Accepted Manuscript* or any consequences arising from the use of any information it contains.

ROYAL SOCIETY OF CHEMISTRY

www.rsc.org/softmatter

Journal Name

ARTICLE TYPE

Cite this: DOI: 10.1039/xxxxxxxxxx

Direct calculation of anisotropic surface stresses during deformation of a particle-covered drop†

Chuan Gu, Lorenzo Botto,[a]

Received Date
Accepted Date

DOI: 10.1039/xxxxxxxxxx

www.rsc.org/journalname

The modification of the surface tension and the surface shear elasticity by particles in particle-covered drops can be attributed to a particle-induced surface stress. This stress represents at the macroscopic, continuum level the microscopic effect of lateral particle-particle interactions. Understanding the link between the isotropic and anisotropic components of the surface stress and the particle microstructure, and how these components change when structured interfaces deform, is a crucial problem in the field of particle-laden interfaces. In this paper we analyse static and transient three-dimensional simulations of a pendant drop whose surface is covered by colloidal particles displaying purely repulsive particle-particle interactions. We compute the isotropic and anisotropic surface stress from the inter-particle forces using a version of the Kirkwood-Irving formula suitable for interfacial suspensions; we validate the approach by comparing against surface tension values obtained with Fordham's method (*Proc. Roy. Soc. London A*, 194, 1948). In the parameter range simulated, the combination of parameters for which the drop does not pinch off (stable drop) gives rise to a homogeneous and isotropic surface stress; we argue that in the absence of attractive interactions the drop becomes unstable before anisotropic effects can manifest themselves. For unstable drops, stress non-uniformity and anisotropy are significant when the drop deformation and the solid area fraction are sufficiently large. Our results have implications for the dynamic deformation of structured interfaces with geometrically complex and time dependent morphologies.

1 Introduction

The use of solid particles that adsorb at fluid interfaces is emerging as a powerful alternative to molecular surfactants in applications such as emulsion, foam and polymer blend stabilisation,[1–4] microfluidics,[5–7] froth flotation,[8], and the design of soft interfacial materials.[9,10] Solid particles display also interesting analogies with globular proteins,[11] which makes the study of particle-covered (or particle-laden) interfaces relevant to the production of food and personal care products. Understanding the mechanisms by which the particles modify the interfacial properties and developing coarse-grained constitutive models that can represent the mechanical response due to the particles in an effective manner remain crucial challenges.[12] The bulk of the literature so far has focused on the effective surface tension, which is related to the isotropic component of the surface stress. The presence of anisotropic surface stresses - which can be induced by flow, external field or confinement[13] - gives rise to interesting effects such the formation of wrinkles[14–19] and plastic interfacial deformations.[20] An improved understanding of how anisotropic stresses relate to the particle distribution could enable to better predict and control these effects. In this work we propose a framework of analysis of surface stresses based on numerical simulations in which the particles are represented as discrete objects and the surface stress is calculated by performing local area averages. We are able to measure *local* isotropic and anisotropic surface stresses in both static drops and dynamically deforming drops. Our simulations provide insights into the link between local surface stress components and the spatial distribution of the particles for a problem in which the interface has a non-trivial morphology.

Solid particles adhere to fluid interfaces owing to a reduction in total surface energy. This energy includes contributions due to the solid-fluid and fluid-fluid interfaces. The difference between the surface energy of the particle in the bulk and in the interface defines the capillary adsorption energy.[21] Such adsorption energy can amount to several million kT for micron-sized particles and is important even for nanoparticles. In interfaces stabilised by colloids, this robust adhesion mechanism is responsible for constraining the suspension to the curved surface of the drop, bubble, polymer blends, *etc.*

The mechanical properties of the composite interface, *i.e.* the two-dimensional "material" composed by the interface and the

[a] *School of Engineering and Materials Science, Queen Mary University of London, E1 4NS, London, UK. E-mail: l.botto@qmul.ac.uk*

particles embedded in it, depend primarily on the surface stresses induced by the particles. For particles that are much larger than the molecules constituting the interface, the surface stress due to the particles embeds the effect of lateral particle-particle interactions (electrostatic interaction, van Der Waals interactions, capillarity, *etc.*)

In this paper we study such stresses in a simulation of a pendant drop in which the interface is covered by a monolayer of repulsive colloidal particles forming a curved 2D colloidal crystal. Colloidal crystals at fluid interfaces have been used as model systems to study topological defects on curved manifolds.[22,23] Colloidal crystals of varying degree of micro structural order often form in systems when the particles are charged.[24] In our simulations, the particle-particle interaction force model is designed to mimic a screened repulsive Coulomb interaction between charged particles. From a fundamental perspective, considering purely repulsive interactions lays the basis for understanding the interplay between repulsive and attractive forces. Experimentally, the behaviour of flat monolayers of charged particles has been examined at oil-water[25–27] and air-water interfaces.[28] The measured surface pressure shows a strong non-linear dependence on the surface coverage, and is affected by polydispersity[27] and clustering effects.[29].

In contrast to previous pendant drop simulations, in which the complex interface is treated as a continuum (see e.g. Ref.[30]), we treat the particles as discrete objects. In simulation, surface stresses due to particles have been investigated for flat[4,31,31,32] or spherical interfaces.[33] Our work aims to highlight challenges in measuring surface stresses from simulated interfaces presenting non-uniform curvature. Pendant drop experiments with interfacial colloids have focused on the change in surface tension upon adsorption,[34,35] changes in morphology due to the incompressibility of the surface layer,[36], and particle expulsion.[37]

Recent years have seen impressive developments in mesoscale discrete particle simulation methods for colloidal particles, such as the lattice Boltzman method,[38] the Immersed Boundary method, Dissipative Particle Dynamics, Rotational Particle Dynamics, Phase-Field Methods[39,40], *etc*. Many of these methods can be applied to multiphase systems involving particles interacting with fluid interfaces.[41] In addition to enable physical insights into aspects of particle adsorption,[35] particle ordering and dynamics in the interface,[42,43] the effect of particle shape on self-assembly,[44–46] and the modification of the interfacial morphology by the particles,[47,48] such sophisticated numerical tools open up the possibility of measuring accurately local mechanical and micro structural properties.

A practical difficulty with particle-resolved methods such as lattice-Boltzmann methods is to reach a realistic separation of scale between the particles and the drops while keeping the computational cost manageable. To overcome these limitations we have developed FIPI ("Fast Interface Particle Interaction" method), a fast discrete-particle simulation method for interfacial colloids. The method enables to simulate realistic systems with thousand of particles while allowing a good scale separation. The method relies on coupling the Navier-Stokes equation to a phase-field model, and therefore can simulate the coupling to flow.

To calculate surface stresses from a simulation of particles adsorbed to the surface of a drop two main approaches can be adopted. For static problems, the conventional approach is to fit the shape of the composite interface to a numerical solution of the non-linear Young-Laplace equation. Since in general the surface stresses are non-uniform and locally anisotropic, this approach provides a "best-fit" to the properties of the entire drop surface (in ref.[16] a shape-fitting procedure that enable to calculate anisotropic stresses has been recently proposed). A second approach is to calculate the local surface stress directly by local spatial averaging, using an extension of Irving-Kirkwood's expression.[49] It is possible to utilise this approach even when the surface microstructure or the drop shape are time dependent. In this paper, both approaches will be adopted, and the results compared when possible.

For bulk suspensions, the mathematical framework underpinning the method of spatial averaging, which is used to "coarse grain" particle-level quantities, is now quite established (see Ref.[50] for a review). In contrast, work on interfacial suspensions where the method of area average is adopted is scarce, and limited to theoretical investigations to derive balance equations.[51–53] We are not aware of published work specifically investigating the use of the method of area average to extract surface stresses from simulations of interfaces having non-uniform and anisotropic curvatures.

In experiments the interfacial curvature is rarely uniform or isotropic, and this affects the particle distribution in a non-trivial way. On a surface of non-uniform curvature the particles will redistribute on the surface, adopting after surface stress relaxation a concentration distribution consistent with the condition of zero tangential forces on the particles. In addition, while in the case of uniform interfacial curvature and uniform microstruture one can average over the entire surface, non-uniform curvatures necessarily require applying local averaging.

In this paper, following work on bulk suspensions,[54–56] we derive an expression for the interfacial stress similar to Irving and Kirkwood's expression by considering a tangential stress balance and using a Taylor expansion of the surface averaging filter function. Irving and Kirkwood originally derived their formula for the bulk stress by considering the forces between molecules across an element of surface and using an expansion of the density-density correlation.[57] The derivation we propose is easier to interpret in terms of colloidal interactions and makes the link between interfacial stresses and inter-particle forces clearer. For instance, our derivation shows that for pair-wise interactions, the fact that lateral forces can be expressed as the divergence of a stress results from Newton's action-reaction principle. We demonstrate through numerical experiments that the isotropic contribution to the stress calculated from the Irving-Kirkwood expression converges to the surface tension calculations based on fitting the shape of the interface to the Young-Laplace equation. In addition, the Irving-Kirkwood formula enables the direct calculation of the anisotropic (or deviatoric) component of the surface stress, which is related to the surface shear elasticity. We investigate the spatial distribution and magnitude of the anisotropic surface

stresses in static and transient simulations. As it was recently demonstrated with the use of principles of interfacial continuum mechanics, anisotropy and uniformity are intimately linked, as surfaces with non-uniform stress should also display non-isotropic stress, and vice versa.[16]

2 Simulation method

We simulate a pendant drop covered with a monolayer of identical spherical particles. As in classical pendant drop experiments, the drop is held at the top and deforms under gravity. Simulating this problem requires a numerical method that tracks the shape of the composite interface and the position of each particles. For this purpose, we developed a fast Eulerian-Lagrangian method for interfacial colloids, FIPI, which will be briefly described in the following. The method has been thoroughly validated and its complete analysis will be the subject of a forthcoming publication.

At each time-step, FIPI solves the following set of Eulerian equations:

$$\begin{aligned} \frac{\partial \phi}{\partial t} + \mathbf{u}\cdot\nabla\phi &= \nabla\cdot M\nabla\xi \\ -\nabla p + \mu\nabla^2\mathbf{u} + \rho\mathbf{g} + \xi\nabla\phi &+ \sum_{\alpha=1}^{N_p} \mathbf{F}_\alpha \delta(\mathbf{x}-\mathbf{x}_\alpha) = 0 \\ \nabla\cdot\mathbf{u} &= 0. \end{aligned} \tag{1}$$

This system of equations couple a Cahn-Hilliard equation for the phase variable ϕ to the incompressible Navier-Stokes equations for the fluid velocity $\mathbf{u}(\mathbf{x},t)$, where $\mathbf{x}$ is an Eulerian point and t is time. The momentum equation, which is treated in the low-Reynods number limit, includes a gravitational term $\rho\mathbf{g}$, a gradient term $\propto\nabla\phi$, and a particle forcing term. In the particle forcing term the sum is extended to the N_p particles present in the computational domain.

In the absence of the summation term, eqn (1) is the standard formulation of the phase-field method for a two-phase flow of two immiscible incompressible fluids (see *e.g.* Ref.[58]). The function ξ is the chemical potential, which is prescribed as $\xi = \frac{\lambda}{\varepsilon^2}(\phi^3-\phi) - \lambda\nabla^2\phi$, where λ is the mixing energy parameter. Gradients of the chemical potential drive the formation of a diffuse fluid interface of thickness ε at a rate set by the mobility parameter M.[59] The surface tension of the bare interface is $\sigma_0 = 2\sqrt{2}\varepsilon/3$.

The particle forcing term $\sum_{\alpha=1}^{N_p}\mathbf{F}_\alpha\delta(\mathbf{x}-\mathbf{x}_\alpha)$, which contains delta forces applied at the position of the particles, represents the sum of the forces $\mathbf{F}_\alpha$ per unit volume that each particle α exerts on the surrounding environment. The force $\mathbf{F}_\alpha$ is the sum of two contributions: a hydrodynamic force $\mathbf{F}_\alpha^{hd}$ representing the hydrodynamic drag that particle α exerts on the fluid, and an interface-particle capillary force contribution $\mathbf{F}_\alpha^{ip}$. In contrast to particle-resolved methods, in FIPI both terms are modelled. The hydrodynamic drag is modelled as $\mathbf{F}_\alpha^{hd} = 6\pi\mu a\left(\mathbf{U}_{p,\alpha}-\mathbf{U}_{f,\alpha}\right)$, where a is the particle radius, $\mathbf{U}_{p,\alpha}$ is the particle velocity and $\mathbf{U}_{f,\alpha}$ is the fluid velocity at the particle position. The interface-particle interaction term is modelled as

$$\mathbf{F}_\alpha^{ip} = \begin{cases} A\pi\sigma_0 d\mathbf{n}, & \text{if } |\phi(\mathbf{x}_\alpha,t)| \le \phi^* \\ \mathbf{0}, & \text{if } |\phi(\mathbf{x}_\alpha,t)| > \phi^* \end{cases}, \tag{2}$$

where $\mathbf{0}$ is the null vector, $\mathbf{n}$ is the unit normal vector from the interface to the particle center, d is the minimum distance between the particle centre and the interface, and A is a parameter that characterises the magnitude of the capillary adhesion force. The interface-particle interaction force model in eqn (2) gives a potential well centered at the interface that drives the adsorption of each particle and keeps the particle in the interface. The interface-particle interaction force is truncated when the phase-field variable evaluated at the particle position, $\phi(\mathbf{x}_\alpha,t)$, is larger in magnitude than a specified truncation parameter ϕ^*.

In the current implementation of FIPI, the mapping between $\phi(\mathbf{x}_\alpha,t)$ and d is given by the formula $d = \left|\frac{\sqrt{2}}{2}\varepsilon\log\frac{1+\phi(\mathbf{x}_\alpha,t)}{1-\phi(\mathbf{x}_\alpha,t)}\right|$. This formula is obtained by inverting the static one-dimensional solution of the Cahn-Hilliard equation. The interface-particle interaction force in eqn (2) is truncated when $|\phi(\mathbf{x}_\alpha,t)|$ is larger than $\phi^* = 0.964$; this value for the truncation parameter corresponds to $d = 2\sqrt{2}\varepsilon$.

The position of each particle can be calculated by taking into account that the sum of $\mathbf{F}_\alpha^{ip}$ and $\mathbf{F}_\alpha^{hd}$ must balance the inertia of the particle, the particle weight, and the force $\mathbf{F}_\alpha^{pp}$ due to non-hydrodynamic particle-particle interactions. Neglecting particle inertia and weight, Newton's equation of motion for each particle reads $-6\pi\mu a\left(\mathbf{U}_{p,\alpha}-\mathbf{U}_{f,\alpha}\right) - \mathbf{F}_\alpha^{ip} + \mathbf{F}_\alpha^{pp} = 0$. Given a current configuration of the particles, and the velocity and phase fields, Newton's equation of motion is solved to calculate the new position of each particle.

Through the particle forcing term, the particles produce a modification of the mechanical properties of the interface. The term $\xi\nabla\phi$ produces the Laplace pressure due to the bare interface. The term $\sum_{\alpha=1}^{N_p}\mathbf{F}_\alpha\delta(\mathbf{x}_\alpha-\mathbf{x}_s)$ gives an extra Laplace pressure on the interface due to the particles, thus providing a means to change the surface stress. The solution of the Eulerian equations (1) for the fluid and the interface coupled with the particles' equation of motion, gives at each time step the shape of the interface modified by the presence of the particles.

The conservative force on particle α due to particle β is assumed to be repulsive, with a screening length κ^{-1}:

$$\mathbf{F}_{\alpha\beta}^{pp} = \begin{cases} \left(\frac{F_0}{r^2}\right)\hat{\mathbf{r}}, & \text{if } a < r \le \kappa^{-1} \\ \mathbf{0}, & \text{if } r > \kappa^{-1} \end{cases}, \tag{3}$$

Here r is the distance between particles β and α, and $\hat{\mathbf{r}}$ is the unit vector pointing from particle β to particle α. The total force on particle α is obtained by summing over all the particles within the interaction range. The parameter F_0 defines the characteristic magnitude of the inter-particle force.

The force law in eqn (3) represents a model for a screened Coulomb interaction between charged colloids (κ^{-1} models a finite Debye length). Coulomb and dipole-dipole electrostratic interaction forces between colloids at fluid-fluid interface can

be approximated by power laws with r^{-2} and a r^{-4} decay, respectively.[22,60–62] In addition to be relevant to experiments with strongly charged particles,[22] the r^{-2} law makes particle-particle interaction effects more marked, and therefore was chosen for the current work. It is expected that the qualitative features of the results presented in the current paper will not depend significantly on the value of the power-law exponent.

The governing equations are solved in a triply-periodic domain by a pseudo-spectral method. Spectral methods enables accurate evaluation of spatial derivatives owing to the Fourier series representation, and a fast numerical solution. To pin the drop at its top portion, we use a ring of stationary particles exerting a force in the upward direction, opposite to gravity. For these particles, the particle-interface capillary adhesion was tuned so that the particle ring could sustain the total weight of the drop.

3 Simulation parameters and procedure

The physical parameters related to the fluid and the bare interface are the gravity constant g, the density difference $\Delta\rho$ between the drop and the surrounding fluid, the surface tension of the bare interface σ_0, and the initial radius of the drop R. The parameters associated to the particles are the particle radius a, the number of particles N_p, the inter-particle force parameter F_0, and the cut-off length κ^{-1}. These parameters enable to build the following non-dimensional groups: the area fraction ϕ_s, the Bond number $\mathscr{B} = \Delta\rho g R^2/\gamma_0$ of the drop without the particles, the non-dimensional interaction strength parameter $\mathscr{F} = F_0/(\sigma_0 a^3)$, the interaction range parameter κa, and the ratio of the particle size to the drop size a/R. For all our simulations, the ratio of the particle radius to the initial drop radius is fixed to $a/R = 0.02$.

The area fraction values reported in the current paper are calculated as $\phi_s = N_p \pi a^2/A_0$, where $A_0 = 4\pi R^2$. Since they are based on the initial drop radius, the values of ϕ_s should be interpreted as nominal area fractions. By calculating the local area fraction at the drop apex by area averaging we have verified that the values of ϕ_s based on the initial drop area are very close numerically to those measured with the deformed drop.

At the start of each simulation, the particles are randomly arranged on the surface of the drop and the inter-particle force is switched off. After enabling the interparticle interactions, the monolayer quickly relaxes to adopt a particle distribution consistent with the instantaneous drop shape. The observed time scale over which the particles relaxed in the interface was found to be much smaller than the time scale of droplet deformation. The microstructure can therefore be assumed to change quasi-statically as the drop deforms.

Unless otherwise specified, the Bond number is $\mathscr{B} = 0.223$, which gives droplet deformations comparable to those seen in pendant drop experiments. For the results shown in Fig.6 and Fig.8 we simulate a larger Bond number, $\mathscr{B} = 0.334$.

The physics of capillary particle adsorption requires the capillary adhesion parameter A to be a constant of O(1), whose exact value depends on the contact angle and on the ratio of the particle size to the drop size.[44,63–65] For static simulations we have used $A = 1$. When using $A = 1$ in transient simulations, under conditions of large surface coverage the particles are expelled from the interface in correspondence to the top edge of the drop. This phenomenon seems to be quite sensitive to the way the drop is pinned. To limit the complexity of our simulations, in transient simulations we constrained the particles to the surface of the drop by choosing $A = 10$.

4 Results

The surface stress tensor evaluated at a generic surface point $\mathbf{x}_s$ due to conservative inter-particle forces can be calculated (see Appendix) as

$$\sigma = \frac{1}{2}\sum_{\alpha=1}^{N_p}\sum_{\beta\neq\alpha}^{N_p} \mathbf{F}_{\alpha\beta}(\mathbf{y}_s^\beta - \mathbf{y}_s^\alpha) G(\mathbf{x}_s - \mathbf{y}_s^\alpha). \tag{4}$$

In this expression, $\mathbf{F}_{\alpha\beta}$ is the force on particle α due to particle β (in eqn 3, the same quantity is denoted by the symbol $\mathbf{F}^{pp}_{\alpha\beta}$). The surface position vectors $\mathbf{y}_s^\alpha$ and $\mathbf{y}_s^\beta$ locate the centers of particles α and β, respectively. The summation is over all the particles in the monolayer. The function G is a smooth surface filter function with compact support that isolates a surface control region around $\mathbf{x}_s$. Typical choices for the filter function suggested by three-dimensional calculations are the box function and the Gaussian filter; the specific choice of filtering should not affect the definition of spatially-average quantities.[54]

In the calculations presented in the current paper, G is a box function, constant and equal to $1/A_c$ in a curved surface element (the averaging region) of area A_c centered at $\mathbf{x}_s$ and zero otherwise. Using index notation, the use of the box function yields the following formula:

$$\sigma_{ij} = \frac{1}{2A_c}\sum_{\alpha}\sum_{\beta\neq\alpha} F_{\alpha\beta,i}(y^\beta_{s,j} - y^\alpha_{s,j}). \tag{5}$$

The derivation presented in the Appendix shows that in this expression the index α runs over all the particles within the averaging region, while β indexes particles that can be either inside or outside the averaging region.

Our derivation of formula (4) follows from recent work on bulk suspensions by Nott, Guazzelli and Pouliquen,[56] who in turn extended work by Anderson and Jackson on suspension stresses due to particle-particle contacts.[54,55] The derivation assumes pairwise interactions; however, the formula is expected to hold more generally.[56] Eqn (4) can be recognised as a version of the Irving-Kirgwood formula, here applied to a system of particles constrained to a curved surface.

The surface stress due to the particles can be decomposed into an isotropic and a deviatoric (anisotropic) component as $\sigma_{ij} = -\Pi_s\delta_{ij} + \sigma^D_{ij}$. The deviatoric component σ^D_{ij} is associated to the shear elasticity of the particle monolayer. The surface pressure Π_s is the stress response due to the particles to an isotropic dilatation or compression of the particle monolayer. In our simulation the surface tension of the bare interface σ_0 affects only the isotropic component of the surface stress of the composite interface (in our simulation the particles are assumed to be much larger than the molecules composing the bare interface).

Taking the trace of eqn (5) and multiplying by $-1/2$ yields the

following formula for the surface pressure due to the particles:

$$\Pi_s = -\frac{1}{4A_c}\sum_{\alpha}\sum_{\beta\neq\alpha}\mathbf{F}_{\alpha\beta}\cdot(\mathbf{y}_s^{\beta}-\mathbf{y}_s^{\alpha}). \quad (6)$$

We here adopt an orthogonal coordinate system (s,θ), where θ denotes the azimuthal coordinate and s the meridian coordinate.[16] Lines at constant s are circles lying in planes perpendicular to the axis of the drop. The local tensions due to the particles in the azimuthal and meridian directions corresponding to eqn (5) are given by

$$\sigma_{\theta\theta} = \frac{1}{2A_c}\sum_{\alpha}\sum_{\beta\neq\alpha}F_{\alpha\beta,\theta}\left(y_{s,\theta}^{\beta}-y_{s,\theta}^{\alpha}\right) \quad (7)$$

and

$$\sigma_{ss} = \frac{1}{2A_c}\sum_{\alpha}\sum_{\beta\neq\alpha}F_{\alpha\beta,s}\left(y_{s,s}^{\beta}-y_{s,s}^{\alpha}\right), \quad (8)$$

respectively.

In our simulation, the surface stress tensor is diagonal in the local coordinate system (θ,s). In other words, lines at constant θ and constant s, which are parallel to the principal directions of curvature, define also the principal directions of surface stress. The surface pressure satisfies $\Pi_s = -(\sigma_{\theta\theta}+\sigma_{ss})/2$. The deviatoric components of the surface stress in the azimuthal and meridian directions are given by $\sigma^D_{\theta\theta} = (\sigma_{\theta\theta}-\sigma_{ss})/2$ and $\sigma^D_{ss} = -\sigma^D_{\theta\theta}$, respectively.

Simulated equilibrium drop shapes for two values of the area fraction are shown in Fig.1. As the number of particles increases (for a fixed particle size), the drop assumes a more elongated shape, suggesting a reduction in the effective surface tension of the composite interface. For the values of area fraction shown, the particles are seen to be arranged in a dominant hexagonal order, forming a 2D colloidal crystal. In Fig.1 (b) a disclination in the crystal structure in which one particle is surrounded by 7 particles is indicated by a circle. Topological defects are important features of hexagonal crystals on curved surfaces.[22,23,66,67]

4.1 Effective surface tension by shape fitting

Denoting by κ_θ and κ_s the local curvatures of the interface along the azimuthal and meridian directions, respectively, the normal stress balance for the composite interface (treated as a two-dimensional continuum) reads[16]

$$\sigma_s\kappa_s + \sigma_\phi\kappa_\theta = p_s. \quad (9)$$

Here σ_ϕ and σ_s are the interfacial tensions in the azimuthal and meridian directions, respectively, and p_s is the pressure difference between the inside and the outside of the drop. For an isotropic stress tensor, $\overline{\sigma} = \sigma_\phi = \sigma_s$ and eqn (9) reduces to the classical form of the Young-Laplace equation:

$$\overline{\sigma}(\kappa_s+\kappa_\theta) = p_s. \quad (10)$$

Since the change in p_s along the composite interface is due to gravity, $p_s = p_0 - \Delta\rho gz$, where p_0 is the value of p_s at the drop apex. The curvatures in the azimuthal and meridional directions can be expressed in terms of the slope angle $\theta = \frac{dz}{dr}$ (r is the distance of from the symmetry axis) as $\kappa_s = \frac{d\theta}{ds}$ and $\kappa_\phi = \frac{\sin\theta}{r}$ giving $\frac{d\theta}{ds} = -\frac{\sin\theta}{r} + \frac{p_0}{\overline{\sigma}} - \frac{\Delta\rho gz}{\overline{\sigma}}$. This equation, together with the definitions $dr = \cos\theta ds$ and $dz = \sin\theta ds$, constitute a closed non-linear system of equations that can be solved numerically.[68] The numerical solution for the drop shape is at the basis of standard pendant drop measurements.[69,70]

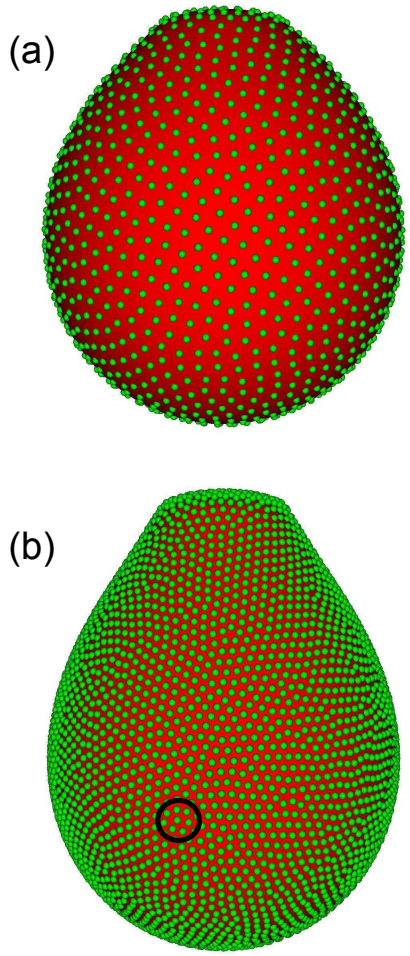

Fig. 1 Steady-state drop shapes for (a) $\phi_s = 0.15$ and (b) $\phi_s = 0.45$; $\mathscr{F} = 0.707$ and $\kappa a = 0.064$.

Fordham[71] showed that when $\overline{\sigma}$ is constant, only two geometric parameters are needed to calculate the surface tension: the maximum diameter of the drop, D_e, and the diameter of the drop at a distance D_e from the apex, D_s. From these two values, the surface tension can be calculated as

$$\overline{\sigma} = \frac{g\Delta\rho D_e^2}{H}, \quad (11)$$

where H is a unique function of the ratio D_s/D_e. In Ref.[71], accurate values for H calculated by solving eqn (10) numerically are tabulated.

We have applied Fordham's method to our simulation data to calculate the effective surface tension of the interface with the particles. To validate the approach, we have calculated the surface tension of the drop without the particles and compared this value to the surface tension prescribed as input parameter to the

phase-field method. In all the cases, the computed results were found to be within 2% from the theoretical surface tension values. Unlike experiments, simulations are subject to very limited noise in the data, so such good accuracy is not unexpected. In the following we often refer to Fordham's method as "shape-fitting method", although what we are fitting is the drop curvature at two selected points, not the actual drop shape.

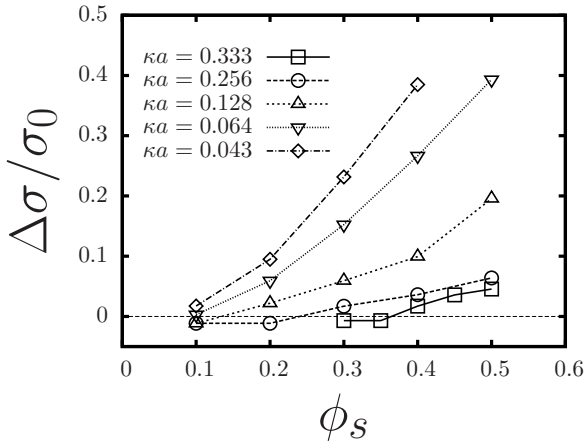

Fig. 2 Surface tension reduction, $\Delta\sigma = \sigma_0 - \overline{\sigma}$, vs. the area fraction for different values of κa; κ^{-1} is the range of the repulsive force and a is the particle radius.

Fig.2 shows the surface tension reduction $\Delta\sigma = \sigma_0 - \overline{\sigma}$, calculated by using Fordham's method, for the particle-laden case. The surface tension was calculated at equilibium, *i.e.* when the drop had reached a steady-state shape. The surface tension reduction is plotted as a function of the area fraction for $\mathscr{F} = 0.707$ and different values of κa. The maximum area fraction we were able to explore with stable drops is $\phi_s = 0.5$ for $\kappa a > 0.043$ and $\phi_s = 0.4$ for $\kappa a = 0.043$. For each value of κa, increasing the area fraction beyond these upper limits led to unstable drops, as discussed below.

As expected for purely repulsive inter-particle forces,[72] the presence of the particles produce a reduction in surface tension ($\Delta\sigma > 0$). The surface tension reduction is seen to increase faster than linearly with ϕ_s. The tension on an element of composite interface along a given direction is given by the force per unit length along that direction. This force is due partly to the bare interface and partly to the interaction between the particles. Accounting for nearest neighbours only, the particle contribution to the tension can be roughly estimated to be proportional to the ratio of interparticle force and interparticle separation. As ϕ_s increases the inter-particle force increases approximately proportionally to ϕ_s (for a $1/r^2$ decay). Since the tension is due to this force acting over a distance roughly comparable to the interparticle separation, then the surface tension should increase more than linearly with ϕ_s. This behaviour is consistent with Fig.2.

The curves referring to relatively large values of κ suggest that the surface tension reduction is very small for a non-zero value of ϕ_s. Because of the finite range of the interparticle force, athermal particles separated by a distance larger than κ^{-1} will not interact with each other, giving no effect of the particles at finite surface coverages. In our case, when the inter particle separation is larger than κ^{-1} the surface tension reduction is not strictly zero, but is nevertheless negligibly small in comparison to typical values of $\Delta\sigma$.

We can develop an estimate of the relation between cut-off length κ^{-1} and the critical area fraction necessary to obtain zero effect of the particles on the surface tension. For particles in hexagonal packing on a planar interface, the average interparticle distance is $\ell = \left(\frac{2\pi a^2}{\sqrt{3}\phi_s}\right)^{1/2}$. Setting $\ell = \kappa^{-1}$ the estimated value of the area fraction for which $\Delta\sigma = 0$ is $\phi_{s,min} = \frac{2\pi}{\sqrt{3}}(\kappa a)^2$. This estimate gives $\phi_{s,min} \simeq 0.4$ for $\kappa a = 0.33$, in reasonable agreement with the values of Fig.2.

As the cut-off distance κ^{-1} approaches the particle diameter, the system approaches the hard disk limit in which the surface tension changes only when the particles are in physical contact. In this limit we expect $\Delta\sigma = 0$ for ϕ_s smaller than the value ≈ 0.92 that corresponds to maximum packing. A signature of this behaviour is the fact that the curves in Fig.2 become flatter as κa increases.

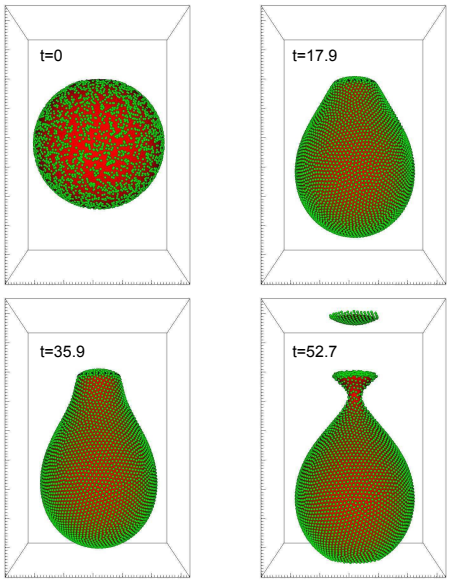

Fig. 3 Time evolution of the drop breakup process for $\phi = 0.5$ and $\kappa a = 0.043$. Time is in units of $\sqrt{R/g}$.

For a fixed value of the non-dimensional force strength parameter $\mathscr{F}$, and a fixed area fraction ϕ_s, the results should not change with the size ratio a/R (provided that this ratio is sufficiently for a reasonable scale separation to hold). This does not mean that there are no particle size effects. Both $\mathscr{F}$ and ϕ_s depend on the size of the particle for a fixed average inter-particle separation.

If the surface tension reduction is larger than a threshold value, the drop becomes unstable and pinches off, as illustrated in Fig.3. Padday and Pitt[73] investigated the stability of axisymmetric menisci. Their results suggest that for our case the critical Bond number separating stable and unstable regions should be about $\mathscr{B} = 0.28$. Noticing that $\Delta\sigma$ increases monotonically with ϕ_s, the results of Fig.2 for $\kappa a = 0.043$ indicate that for $\phi_s = 0.5$ the surface tension reduction should be larger than $0.4\sigma_0$. A reduction in sur-

face tension by more than 40% results in a Bond number larger than 0.37. This value is in the unstable region.

Our simulations refer to phenomena that occur well before pinch off. The effect of interfacial particles on fluid dynamic events occurring at pinch-off is an intriguing phenomenon that has received some attention recently.[74]

4.2 Surface stress by local area averaging

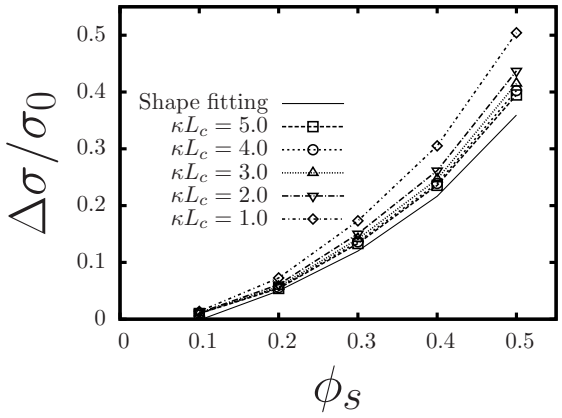

Fig. 4 Surface pressure at the drop apex for different values of κL_c, where L_c is the radius of the averaging control region. The interaction strength parameter is $\mathscr{F} = 1.414$, and $\kappa a = 0.128$. The continuous line corresponds to the values of $\Delta\sigma$ calculated by shape fitting (see Fig.2).

A significant challenge in performing area averaging is choosing the size of the averaging control region. This size must be sufficiently large in comparison to the inter-particle distance and sufficiently small in comparison to the characteristic radius of curvature of the drop. In order not to introduce an artificial cut-off, the size of the control region must also be significantly larger than the interaction range κ^{-1}. This scale separation is ensured in pendant drop experiments, where κ^{-1} is at most a few microns and R is typically of the order of 1mm. In simulation, however, these constraints are more stringent, due to the limited ability of simulations to treat a very large number of particles. When performing average, each choice for the size of the control region represents a compromise, and will introduce some error. This error is expected to decrease as the inter particle separation and the interaction range are reduced with respect to the drop size.

To illustrate how area-averaged results change as a function of the size of the averaging control region, we show in Fig.4 the surface pressure at the drop apex for different values of L_c, where L_c is a parameter characterising the size of the control region. Area averaging is carried out by considering a sphere of radius L_c surrounding the apex; the intersection of such sphere with the drop shape defines a curved surface, having approximately the shape of a spherical cap. The area of this surface is used in the denominator of eqn (5). In Fig.4, the values of $\Delta\sigma$ given by the shape-fitting method are also shown for comparison (solid line).

For an interface having uniform and isotropic surface stress, we expect the values of Π_s to converge to the values of $\Delta\sigma$. Fig.4 shows that as L_c increases the value of Π_s computed by area averaging approaches from above the value of $\Delta\sigma$ calculated with the shape-fitting method. For the parameters explored, a value of L_c larger than about $3\kappa^{-1}$ gives reasonably converged values (this result is in keeping with preliminary tests on a planar monolayer). The absolute deviation between Π_s and $\Delta\sigma$ appears to slightly increase with increasing area fraction. The relative deviation is however roughly constant. Given the incomplete scale separation in our simulation, the agreement between the results of formula 6 and the shape-fitting method is overall reasonably good. For $\kappa L_c = 5$, the relative error is less than 10%. Within a tolerable error, the shape fitting method and the direct calculation of the stress by the Irving-Kirkwood formula thus give approximately the same surface pressure value.

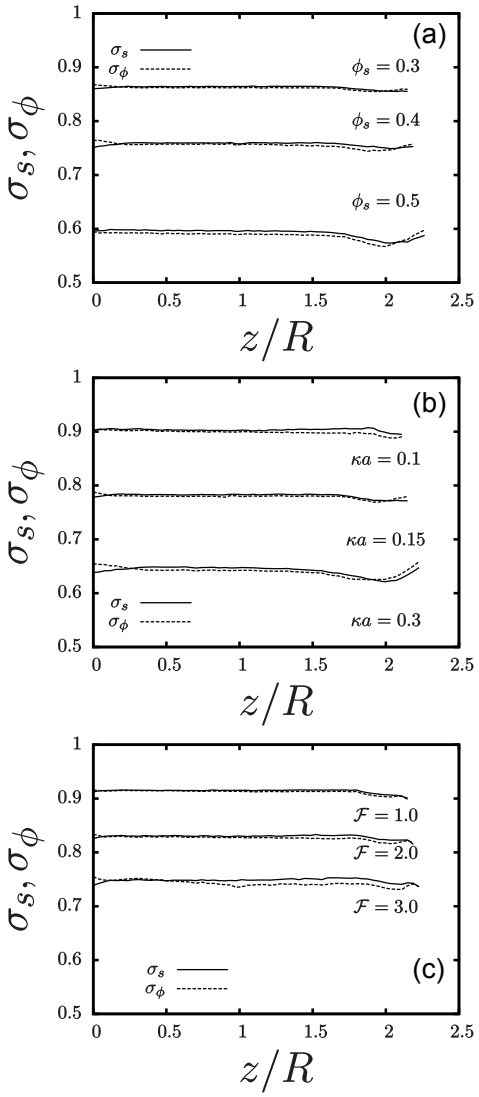

Fig. 5 Azimuthal and meridian tensions for (a) different area fractions and fixed $\mathscr{F} = 1.414$ and $\kappa a = 0.128$; (b) different values of the interaction range and fixed $\phi_s = 0.4$ and $\mathscr{F} = 1.5$; (c) different values of the interaction strength parameter $\mathscr{F}$ and fixed $\phi_s = 0.4$ and $\kappa a = 0.2$. The tensions are normalised by the bare surface tension σ_0.

Fig.5 (a), (b) and (c) show the total azimuthal and meridian tensions, $\sigma_\theta = \sigma_0 + \sigma_{\theta\theta}$ and $\sigma_s = \sigma_0 + \sigma_{ss}$, as a function of the axial coordinate z for a selected range of simulation parameters,

corresponding to different combinations of the parameters $\mathscr{F}$, κa and ϕ_s. The magnitude of the deviatoric stress is given by the spread between the continuous and dashed curves, while the average of these two curves gives the isotropic tension of the composite interface, $\sigma_0 - \Pi_s$. For these result we use an isotropic filter including in the average particles within a sphere of radius $L_c = 4\kappa^{-1}$.

The azimuthal and meridian tensions are seen to be practically constant over the surface of the drop, and very close numerically to each other, suggesting negligible anisotropic effects and practically uniform surface stress. The small fluctuations visible for $z/R > 1.7$ are likely due to edge effects. The distance between the particles located in this region and the ring of particles pinning the drop is comparable to the filter radius, so the filter "picks up" unphysical force values. The general trend suggested by Fig.5 is that increasing $\mathscr{F}$, ϕ_s, or the interaction range gives a larger surface pressure and therefore a smaller tension.

In our simulations the surface stress anisotropy is negligible in the range of parameters in which the drop achieves static equilibrium. We have explored several simulation parameters looking for the range in which anisotropic effects are more marked. We have found that for variations of the simulation parameters in the direction that should give more pronounced anisotropic effects (larger inter particle forces, larger area fraction, and larger deformations), the drop quickly becomes unstable and pinches off. For stable drops, the surface stress is homogeneous and isotropic as in Fig.5.

From a qualitative point of view, this behaviour can be understood from the following argument. In the absence of attractive interactions between the particles, the azimuthal and meridian tensions decrease with increased deformations. To achieve a degree of stress anisotropy sufficiently large to be measured, the inter-particle forces need to be relatively large and the interface sufficiently stretched in the direction of gravity. However, an increase in interparticle forces leads to a surface tension reduction, bringing the system in the range of parameters in which the drop is unstable. Increasing the deformation makes the drop neck narrower, resulting in surface tension forces being unable to support the weight of the drop. Starting from a smaller Bond number, and thus from a smaller initial drop deformation, allows to be farther from the unstable region, but also reduces the anisotropic deformation of the microstructure.

Our results could suggest that in the absence of attractive interactions and for repulsive interactions having a range significantly large in comparison to the particle size, anisotropic stresses in stable pendant drops may be observed only in a very narrow range of parameters.

4.2.1 Transient simulations

In this section we illustrate the emergence of anisotropic effects in transient simulations. In these simulations the drop pinches off on long times , but the drop deformations are sufficiently slow to allow the surface stress to relax. Transient surface stress effects are important as they could control the generation of droplets with complex fluid interfaces in microfluidic or millifluidic devices.[13] For experiments with millimeter-sized drops, the experimental time-scale of gravity-induced pinching illustrated in this section is roughly 0.1 seconds.

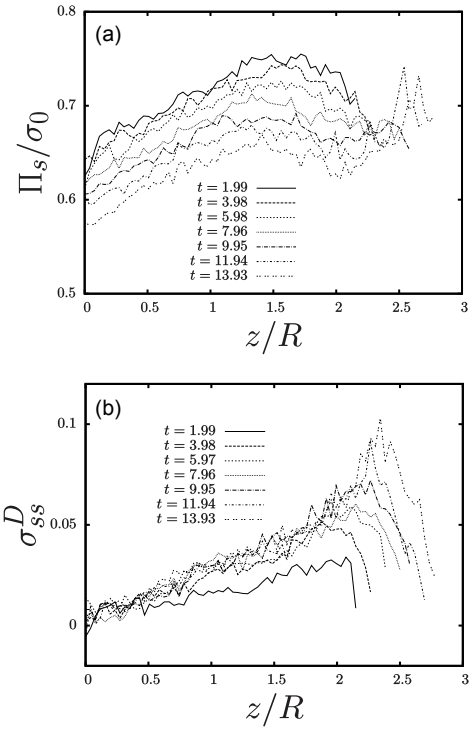

Fig. 6 Time evolution of the surface pressure, (a), and deviatoric meridian surface stress, (b), for $\phi_s = 0.7$, $\kappa a = 0.4$ and $\mathscr{F} = 6.0$. The origin of the axial coordinate z is the drop apex. Time is in units of $\sqrt{R/g}$.

Figs.6 (a) and (b) show the time evolution of the surface pressure Π_s and the meridian component of the deviatoric surface stress σ^D_{ss}, respectively, for a relatively short-ranged interaction, $\kappa^{-1} = 2.5a$. The area fraction and interaction strength parameters are $\phi_s = 0.7$ and $\mathscr{F} = 6.0$, respectively. Contours of the corresponding drop shapes, shown in Fig.7, illustrate how the drop shape changes as time progresses.

Owing to the drop deformation and corresponding dilatation of the interface, the surface pressure decreases in time. In the region $z/R < 2.0$, and sufficiently above the drop apex, σ^D_{ss} increases for $t < 4.0$ and then remains approximately constant. This observation is consistent with the change in shape of the drop suggested by the contour plots of Fig.6(c): after an initial transient the bottom part of the pendant drop reaches an almost stationary shape that translates downward as a neck gradually forms in the region adjacent to the top edge of the drop. The deviatoric stress is zero at the apex and increases with z. This suggests that the monolayer in the bottom part of the drop expands approximately isotropically with time, while the drop side deforms in an anisotropic manner.

Figure 8 (a) shows the surface pressure corresponding to a fixed time, $t = 9.95\sqrt{R/g}$, for three selected cases, labelled "A"," B" and "C". The corresponding total tensions in the azimuthal and meridian directions are shown in Fig.8 (b). The three cases "A"," B" and "C" correspond to $\phi_s = 0.5, 0.55$ and 0.7, respectively. The interaction range and interaction strength parameters are as in Fig.6.

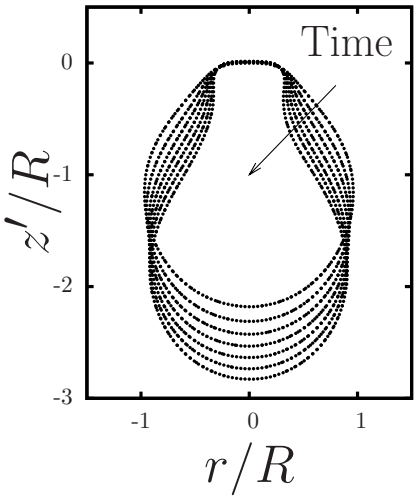

Fig. 7 Contours of the drop shapes corresponding to the seven time instants of Fig. 6. Here z' is an axial coordinate with origin at the top edge of the drop.

Case "A" illustrates a situation in which the surface stress is approximately isotropic, while effects of anisotropy are significant in cases "B" and "C". For a fixed time, therefore, the degree of stress anisotropy increases with increasing surface coverage. The azimuthal component of the surface stress is smaller than the meridian component for any value of z. The degree of anisotropy, negligible in the near-apex region (because of the axial symmetry, the surface stress must be strictly isotropic at the drop apex), becomes more marked as z increases. For z slightly larger than $2R$, the absolute difference between σ_θ and σ_s appears to decrease slightly. However, it is likely that the values in this region are contaminated by edge effects due to the averaging region overlapping partially with the top edge of the drop.

Snapshots of the local microstructure of the monolayer corresponding to cases "A", and"C" are shown in Fig.9. For each case, two snapshots are shown: one referring to the apex region and one referring to the neck region (*i.e.* to the side region where the drop diameter decrease in time). In the apex region, the microstructure is seen to be approximately isotropic, while the neck of the drop is on average characterised by a smaller inter-particle distance in the horizontal direction (the azimuthal direction) than in the vertical direction. Deviations from an hexagonal arrangement are evident. The smaller inter-particle distance in the azimuthal direction gives rise to a larger repulsive force in this direction. This can explain why σ_θ is smaller than σ_s.

Some of the qualitative features of the curves described in cases "B" and "C" are similar to those discussed in a recent paper by Danov *et al.* [16], where anisotropic stresses where measured. This paper reports on experiments with buoyant bubbles in contact with a solution of HFBII, a small compact protein molecule; upon adsorption to fluid interfaces, HFBII produces rigid layers displaying a measurable surface shear elasticity. In qualitative agreement with the results of Fig.8, Danov *et al.* found that σ_s was larger than σ_θ for any given value of z, and that the magnitude of the

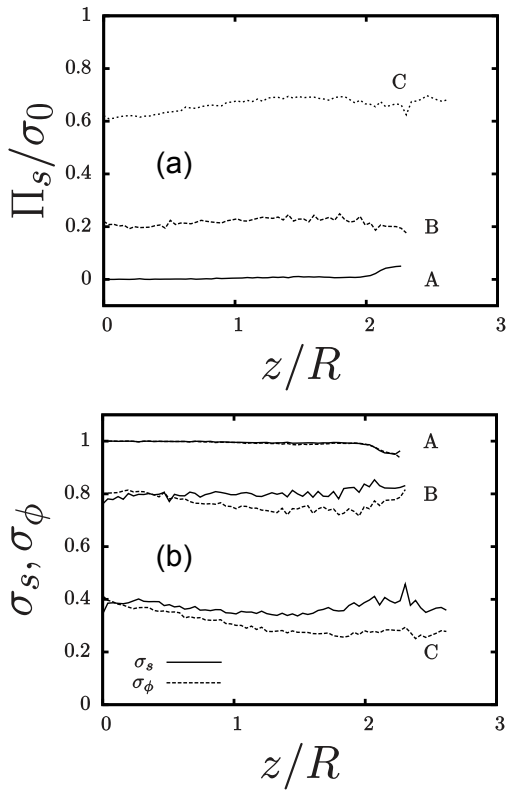

Fig. 8 (a) Surface pressure and (b) total meridian and azimuthal tensions as a function of the axial coordinate for $t = 9.95\sqrt{R/g}$ and $\phi_s = 0.5$ (case A), $\phi_s = 0.55$ (case B) and $\phi_s = 0.7$ (case C).

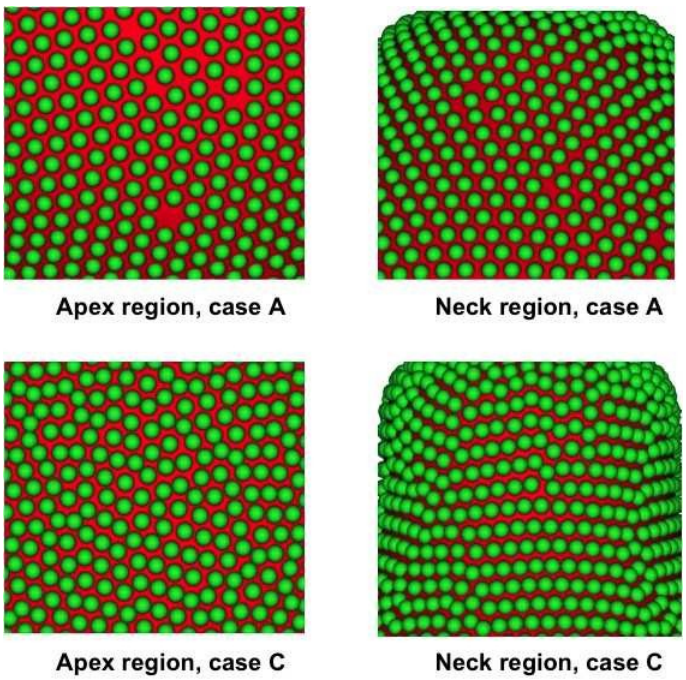

Fig. 9 Snapshots of the monolayer microstructure in the drop apex region and neck region for cases (A) and (C).

deviatoric stress increased with z for locations not too close to the lower boundary of the bubble. A possible difference between our case and the case examined by Danov and collaborators is that in our case the "bonds" between the particles become weaker as they are stretched (purely repulsive interaction), while in that experimental case some form of short-ranged cohesion between the protein molecules is expected. As a note of caution, proteins at interfaces may behave differently from solid particles owing to changes in configuration of the proteins upon contact with the interface. Our comparison is therefore purely qualitative. Some of the effects observed with proteins could be modelled with lumped approaches by extending the numerical model presented in the current paper.

5 Conclusions

We performed a simulation of a pendant drop presenting an interface covered with repulsive spherical particles. We analysed the distribution of the surface stress and examined how the components of this tensor change as a function of selected governing parameters. The main parameters explored in this study are the area fraction, the inter-particle interaction strength parameter, and the interaction range. We presented results for both static and dynamic drop shapes.

For the range of simulated parameters for which the drop had a stable shape, the surface stress was found to be practically isotropic. Anisotropic effects were measurable only in transient simulations, and at relatively high values of the area fraction. In transient simulations, anisotropic effects were more marked along the sides of the drop, corresponding approximately to the neck region where eventually the drop pinches off. In the case of highly deformed drops, visualisations of the microstructure of the monolayer highlighted marked deviations from an hexagonal arrangement.

In this work the surface stress was calculated by local area averaging, using a formula that is analogous to the Irving-Kirkwood formula of molecular dynamics. Reasonably good agreement was found between the predictions for the surface pressure given by this formula and the surface tension reduction calculated by evaluating the interface curvature at two points and fitting to a solution of the Young-Laplace equation (method of Fordham,[71]).

By giving insights into the local microstructure/surface stress relation, our simulation approach could be used to analyse experimental pendant drop data. For instance, the simulated shape of the drop could be fitted to the experiental shape by tuning the inter-particle pair potential to obtain information on colloidal interactions at interfaces. While results for curved surfaces are more difficult to interpret than those obtained on a planar surface, they are also more realistic, as they account for the two-way coupling between particle distribution and interface shape.

In our simulations we have constrained the particles to lie on the surface of the drop. However, increasing the inter-particle forces beyond a certain threshold can cause particle expulsion,[8,19,37,47] a feature that we have not explored here.

Our simulation approach enables to track the trajectory of each single particle. Simulations in which the particles are represented as discrete elements are exceedingly useful when interfacial constitutive equations are not available. This occurs, for instance, when the interfacial suspensions is polydispersed or particle adsorption changes the surface tension on a time scale comparable to that of the drop deformation. For suspensions having a narrow size distribution (say, for standard deviations of particle size approximately 10% of the mean value) the predictions of this paper for monodispersed suspensions are expected to hold approximately. However, experimental studies on flat monolayers show that when there is a significant disparity between the size of the particles, clustering and segregation phenomena produce a complex dependency of surface pressure on size and concentration ratios.[27] The numerical method presented in this work is ideally suited to studying polydispersity effects and other phenomena (*e.g.*, monolayer fracture and dislocation dynamics) on curved monolayers.

The development of accurate simulation of particles adhered to geometrically complex and time-dependent interface morphologies opens new research opportunities in areas such as interfacial rheology, microfluidic generation of drops and bubbles with structured interfaces, and production of anisotropic Pickering emulsions.

6 Acknowledgement

We thank V. Garbin and A. Striolo for useful discussions. Financial support from the European Community through Career Integration Grant FLOWMAT "Flow and Capillarity in Materials Science" (n. 618335) is acknowledged.

7 Appendix

In analogy to the three-dimensional case,[50] the area average of a continuous quantity f at the surface point $\mathbf{x}_s$ can be defined as

$$\langle f \rangle (\mathbf{x}_s) = \int_\Omega f(\mathbf{y}_s) G(\mathbf{x}_s - \mathbf{y}_s) dA_{\mathbf{y}_s}. \tag{12}$$

Here the surface points $\mathbf{x}_s$ and $\mathbf{y}_s$ belong to the set Ω representing the total surface of the composite interface. The function G is a scalar filter function with compact support in a control region surrounding $\mathbf{x}_s$; G is assumed to be a regular function with suitable properties of smoothness.[54,55] The filter function is normalised so that $\int_\Omega G(\mathbf{x}_s - \mathbf{y}_s) dA_{\mathbf{y}_s} = 1$.

The definition of the surface stress tensor follows from the balance of the forces acting on the particles in the direction tangential to the composite interface. Let $\mathbf{F}_\alpha$ denote the net tangential force acting on a particle located at position $\mathbf{y}_s^\alpha$. From eqn (12), the area-averaged tangential force acting on the particles contained in an area element of particle monolayer centered at $\mathbf{x}_s$ can be expressed as $\langle \mathbf{F} \rangle = \int_\Omega \sum_{\alpha=1}^{N_p} \mathbf{F}_\alpha \delta(\mathbf{y}_s - \mathbf{y}_s^\alpha) G(\mathbf{x}_s - \mathbf{y}_s) dA_{\mathbf{y}_s}$, or equivalently as $\langle \mathbf{F} \rangle = \sum_{\alpha=1}^{N_p} \mathbf{F}_\alpha G(\mathbf{x}_s - \mathbf{y}_s^\alpha)$. The area-averaged tangential force at a surface point is thus a weighted average of the force acting on the particles surrounding that point. The averaging weight is given by the filter function evaluated at the center of each particle.

For pairwise interactions, $\mathbf{F}_\alpha = \mathbf{F}_\alpha^e + \sum_{\beta \neq \alpha} \mathbf{F}_{\alpha\beta}$. Here $\mathbf{F}_\alpha^e$ is the force due to an external field (*e.g.* the particle weight) or to particle inertia, and the summation term is the sum of the conservative forces on particle α due to the other particles. Substituting

this decomposition in the expression for the average force derived above yields

$$\langle \mathbf{F} \rangle = \langle \mathbf{F}^e \rangle + \sum_{\alpha=1}^{N_p} \sum_{\beta \neq \alpha}^{N_p} \mathbf{F}_{\alpha\beta} G(\mathbf{x}_s - \mathbf{y}_s^\alpha). \quad (13)$$

Newton's action-reaction principle requires $\mathbf{F}_{\alpha,\beta} = -\mathbf{F}_{\beta,\alpha}$. However, because particles α and β are weighted differently by the filter function according to their location, the forces in the summation term of eqn (13) do not cancel out identically. To exploit the symmetry introduced by the action-reaction principle, we perform a Taylor expansion of the filter function about the location of particle α:

$$G(\mathbf{x}_s - \hat{\mathbf{y}}_s^{\alpha\beta}) \simeq G(\mathbf{x}_s - \mathbf{y}_s^\alpha) + \nabla_{\mathbf{y}_s} G(\mathbf{x}_s - \mathbf{y}_s^\alpha) \cdot (\hat{\mathbf{y}}_s^{\alpha\beta} - \mathbf{y}_s^\alpha), \quad (14)$$

where $\hat{\mathbf{y}}_s^{\alpha\beta}$ denotes the midpoint between particles α and β. Using this expansion in eqn (13) the inter-particle interaction term can be written as

$$\sum_{\alpha=1}^{N_p} \sum_{\beta \neq \alpha}^{N_p} \mathbf{F}_{\alpha\beta} G(\mathbf{x}_s - \mathbf{y}_s^\alpha) =$$

$$\sum_{\alpha=1}^{N_p} \sum_{\beta \neq \alpha}^{N_p} \mathbf{F}_{\alpha\beta} G(\mathbf{x}_s - \hat{\mathbf{y}}_s^{\alpha\beta}) - \nabla_{\mathbf{y}_s} \cdot \sum_{\alpha=1}^{N_p} \sum_{\beta \neq \alpha}^{N_p} \mathbf{F}_{\alpha\beta} (\hat{\mathbf{y}}_s^{\alpha\beta} - \mathbf{y}_s^\alpha) G(\mathbf{x}_s - \mathbf{y}_s^\alpha). \quad (15)$$

Since $\hat{\mathbf{y}}_s^{\alpha\beta} = \hat{\mathbf{y}}_s^{\beta\alpha}$, the first double summation on the right-hand side of eqn (15) is identically zero. Thus

$$\sum_{\alpha=1}^{N_p} \sum_{\beta \neq \alpha}^{N_p} \mathbf{F}_{\alpha\beta} G(\mathbf{x}_s - \mathbf{y}_s^\alpha) =$$

$$\nabla_{\mathbf{x}_s} \cdot \left[\frac{1}{2} \sum_{\alpha=1}^{N_p} \sum_{\beta \neq \alpha}^{N_p} \mathbf{F}_{\alpha\beta} (\mathbf{y}_s^\beta - \mathbf{y}_s^\alpha) G(\mathbf{x}_s - \mathbf{y}_s^\alpha) \right], \quad (16)$$

where we have used the fact that $\hat{\mathbf{y}}_s^{\alpha\beta} = (\mathbf{y}_s^\alpha + \mathbf{y}_s^\beta)/2$ and $\nabla_{\mathbf{x}_s} = -\nabla_{\mathbf{y}_s}$. The expression in square parenthesis in eqn (16) defines the surface stress due to the particles appearing in eqn (4), correct up to the first order in the inter-particle separation.

References

1 B. P. Binks, *Current Opinion in Colloid & Interface Science*, 2002, **7**, 21–41.

2 Y. Chevalier and M.-A. Bolzinger, *Colloids and Surfaces A: Physicochemical and Engineering Aspects*, 2013, **439**, 23–34.

3 J. Vermant, S. Vandebril, C. Dewitte and P. Moldenaers, *Rheologica acta*, 2008, **47**, 835–839.

4 V. Garbin, I. Jenkins, T. Sinno, J. C. Crocker and K. J. Stebe, *Phys. Rev. Lett.*, 2015, **114**, 108301.

5 K. Edmond, A. Schofield, M. Marquez, J. Rothstein and A. Dinsmore, *Langmuir*, 2006, **22**, 9052–9056.

6 M. K. Mulligan and J. P. Rothstein, *Langmuir*, 2011, **27**, 9760–9768.

7 A. P. Kotula and S. L. Anna, *Soft Matter*, 2012, **8**, 10759–10772.

8 G. Bournival, S. Ata and E. J. Wanless, *Advances in colloid and interface science*, 2015.

9 J. W. Tavacoli, J. H. Thijssen, A. B. Schofield and P. S. Clegg, *Advanced Functional Materials*, 2011, **21**, 1949–1949.

10 J.-Y. Leong, B.-T. Tey, C.-P. Tan and E.-S. Chan, *ACS applied materials & interfaces*, 2015, **7**, 16169–16176.

11 P. Cicuta, E. J. Stancik and G. G. Fuller, *Physical review letters*, 2003, **90**, 236101.

12 A. M. Luo, L. M. Sagis, H. C. Öttinger, C. De Michele and P. Ilg, *Soft matter*, 2015, **11**, 4383–4395.

13 P. Fischer and P. Erni, *Current Opinion in Colloid & Interface Science*, 2007, **12**, 196–205.

14 P. Erni, H. A. Jerri, K. Wong and A. Parker, *Soft Matter*, 2012, **8**, 6958–6967.

15 E. Aumaitre, S. Knoche, P. Cicuta and D. Vella, *The European Physical Journal E*, 2013, **36**, 1–5.

16 K. D. Danov, R. D. Stanimirova, P. A. Kralchevsky, K. G. Marinova, N. A. Alexandrov, S. D. Stoyanov, T. B. Blijdenstein and E. G. Pelan, *Journal of colloid and interface science*, 2015, **440**, 168–178.

17 L. Vaccari, D. B. Allan, N. Sharifi-Mood, A. R. Singh, R. L. Leheny and K. J. Stebe, *Soft Matter*, 2015, **11**, 6062–6074.

18 T. D. Kassuga and J. P. Rothstein, *Journal of colloid and interface science*, 2015, **448**, 287–296.

19 S. Razavi, K. D. Cao, B. Lin, K. Y. C. Lee, R. S. Tu and I. Kretzschmar, *Langmuir*, 2015, **31**, 7764–7775.

20 A. B. Subramaniam, M. Abkarian, L. Mahadevan and H. A. Stone, *Langmuir*, 2006, **22**, 10204–10208.

21 L. Botto, E. P. Lewandowski, M. Cavallaro and K. J. Stebe, *Soft Matter*, 2012, **8**, 9957–9971.

22 W. T. Irvine, V. Vitelli and P. M. Chaikin, *Nature*, 2010, **468**, 947–951.

23 W. T. Irvine and V. Vitelli, *Soft Matter*, 2012, **8**, 10123–10129.

24 X. Zhang, H. Sun and S. Yang, *The Journal of Physical Chemistry C*, 2012, **116**, 19018–19024.

25 R. Aveyard, J. H. Clint, D. Nees and V. N. Paunov, *Langmuir*, 2000, **16**, 1969–1979.

26 S. Reynaert, P. Moldenaers and J. Vermant, *Langmuir*, 2006, **22**, 4936–4945.

27 C. Monteux, J. Kirkwood, H. Xu, E. Jung and G. G. Fuller, *Physical Chemistry Chemical Physics*, 2007, **9**, 6344–6350.

28 P. V. Petkov, K. D. Danov and P. A. Kralchevsky, *Langmuir*, 2014, **30**, 2768–2778.

29 P. V. Petkov, K. D. Danov and P. A. Kralchevsky, *Journal of colloid and interface science*, 2015.

30 S. Knoche, D. Vella, E. Aumaitre, P. Degen, H. Rehage, P. Cicuta and J. Kierfeld, *Langmuir*, 2013, **29**, 12463–12471.

31 N. Fenwick, F. Bresme and N. Quirke, *The Journal of Chemical Physics*, 2001, **114**, 7274–7282.

32 C. Powell, N. Fenwick, F. Bresme and N. Quirke, *Colloids and Surfaces A: Physicochemical and Engineering Aspects*, 2002, **206**, 241–251.

33 H. Fan and A. Striolo, *Physical Review E*, 2012, **86**, 051610.

34 K. Du, E. Glogowski, T. Emrick, T. P. Russell and A. D. Dinsmore, *Langmuir*, 2010, **26**, 12518–12522.

35 L. Isa, E. Amstad, K. Schwenke, E. Del Gado, P. Ilg, M. Kröger and E. Reimhult, *Soft Matter*, 2011, **7**, 7663–7675.

36 H. Xu, S. Melle, K. Golemanov and G. Fuller, *Langmuir*, 2005, **21**, 10016–10020.

37 V. Garbin, J. C. Crocker and K. J. Stebe, *Langmuir*, 2011, **28**, 1663–1667.

38 F. Günther, F. Janoschek, S. Frijters and J. Harting, *Computers & Fluids*, 2013, **80**, 184–189.

39 Y. J. Choi and P. D. Anderson, *International Journal for Numerical Methods in Fluids*, 2012, **69**, 995–1015.

40 T.-L. Cheng and Y. U. Wang, *Journal of colloid and interface science*, 2013, **402**, 267–278.

41 R. van der Sman and M. Meinders, *Advances in colloid and interface science*, 2014, **211**, 63–76.

42 X.-C. Luu, J. Yu and A. Striolo, *Langmuir*, 2013, **29**, 7221–7228.

43 K. Schwenke, L. Isa and E. Del Gado, *Langmuir*, 2014, **30**, 3069–3074.

44 L. Botto, L. Yao, R. Leheny and K. Stebe, *Soft Matter*, 2012, **8**, 4971–4979.

45 L. Yao, L. Botto, M. Cavallaro Jr, B. J. Bleier, V. Garbin and K. J. Stebe, *Soft Matter*, 2013, **9**, 779–786.

46 X.-C. Luu and A. Striolo, *The Journal of Physical Chemistry B*, 2014, **118**, 13737–13743.

47 E. Kim, K. Stratford, R. Adhikari and M. Cates, *Langmuir*, 2008, **24**, 6549–6556.

48 F. Günther, S. Frijters and J. Harting, *Soft matter*, 2014, **10**, 4977–4989.

49 J. S. Rowlinson and B. Widom, *Molecular theory of capillarity*, Courier Corporation, 2013.

50 D. A. Drew, *Annual Review of Fluid Mechanics*, 1983, **15**, 261–291.

51 A. R. Deemer and J. C. Slattery, *International Journal of Multiphase Flow*, 1978, **4**, 171–192.

52 W. Gray and S. Hassanizadeh, *International Journal of Multiphase Flow*, 1989, **15**, 81–95.

53 G. M. Mavrovouniotis and H. Brenner, *Philosophical Transactions of the Royal Society of London A: Mathematical, Physical and Engineering Sciences*, 1993, **345**, 165–207.

54 T. B. Anderson and R. Jackson, *Industrial & Engineering Chemistry Fundamentals*, 1967, **6**, 527–539.

55 R. Jackson, *Chemical Engineering Science*, 1997, **52**, 2457–2469.

56 P. R. Nott, E. Guazzelli and O. Pouliquen, *Physics of Fluids (1994-present)*, 2011, **23**, 043304.

57 J. Irving and J. G. Kirkwood, *The Journal of chemical physics*, 1950, **18**, 817–829.

58 V. Badalassi, H. Ceniceros and S. Banerjee, *Journal of Computational Physics*, 2003, **190**, 371 – 397.

59 D. M. Anderson, G. B. McFadden and A. A. Wheeler, *Annual Review of Fluid Mechanics*, 1998, **30**, 139–165.

60 A. J. Hurd, *Journal of Physics A: Mathematical and General*, 1985, **18**, L1055.

61 A. Moncho-Jordá, F. Martínez-López, A. González and R. Hidalgo-Alvarez, *Langmuir*, 2002, **18**, 9183–9191.

62 B. J. Park, J. P. Pantina, E. M. Furst, M. Oettel, S. Reynaert and J. Vermant, *Langmuir*, 2008, **24**, 1686–1694.

63 O. Pitois and X. Chateau, *Langmuir*, 2002, **18**, 9751–9756.

64 R. Ettelaie and S. V. Lishchuk, *Soft matter*, 2015, **11**, 4251–4265.

65 N. Sinn, M. Alishahi and S. Hardt, *Journal of colloid and interface science*, 2015, **458**, 62–68.

66 M. J. Bowick, L. Giomi, H. Shin and C. K. Thomas, *Physical Review E*, 2008, **77**, 021602.

67 M. J. Bowick and L. Giomi, *Advances in Physics*, 2009, **58**, 449–563.

68 C. E. Stauffer, *The journal of physical chemistry*, 1965, **69**, 1933–1938.

69 S.-Y. Lin, L.-J. Chen, J.-W. Xyu and W.-J. Wang, *Langmuir*, 1995, **11**, 4159–4166.

70 B. Song and J. Springer, *Journal of colloid and interface science*, 1996, **184**, 64–76.

71 S. Fordham, Proceedings of the Royal Society of London A: Mathematical, Physical and Engineering Sciences, 1948, pp. 1–16.

72 H. Fan and A. Striolo, *Soft Matter*, 2012, **8**, 9533–9538.

73 J. Padday and A. Pitt, *Philosophical Transactions of the Royal Society of London A: Mathematical, Physical and Engineering Sciences*, 1973, **275**, 489–528.

74 K. W. Connington, M. Z. Miskin, T. Lee, H. M. Jaeger and J. F. Morris, *International Journal of Multiphase Flow*, 2015, **76**, 32–46.